Rapid Communication

J. Biochem. **136**, 427–431 (2004)
DOI: 10.1093/jb/mvh140

Essential Residues, W177 and R198, of LukF for Phosphatidylcholine-Binding and Pore-Formation by Staphylococcal γ-Hemolysin on Human Erythrocyte Membranes

Naota Monma[1], Vananh T. Nguyen[1], Jun Kaneko[1], Hideo Higuchi[2] and Yoshiyuki Kamio[1,*]

[1]Department of Microbial Biotechnology, Graduate School of Agricultural Science, Tohoku University, Sendai 981-8555; and [2]Center for Interdisciplinary Research, Tohoku University, Sendai 980-8579

Received June 24, 2004; accepted July 21, 2004

LukF and Hlg2 of staphylococcal γ-hemolysin assemble into hetero-oligomeric pores on human red blood cells (HRBC). Here, we demonstrate, using a single-molecule imaging technique, that a W177T/R198T mutant of LukF, which exhibits no binding activity toward phosphatidylcholine, could form intermediate oligomers with Hlg2, including dimers, tetramers, and hexamer/heptamers, on HRBC. But, the mutant neither caused K^+ efflux nor lysed HRBC, indicating that functional pores were not formed. Hence, we conclude that the W177 and R198 residues are essential for proper pore-formation by staphylococcal γ-hemolysin. We also suggest that the interaction between the W177 and R198 residues, and phosphatidylcholine on membranes is the key to the formation of functional pores.

Key words: bi-component cytolysin, hetero-heptameric pore, membrane binding, staphylococcal γ-hemolysin, single-FRET.

Staphylococcal γ-hemolysin has been isolated as a two-component pore-forming cytolysin from *Staphylococcus aureus*, consisting of LukF and Hlg2 (HS) (*1*). These components assemble on the membranes of mammalian erythrocytes into ring-shaped hetero-heptamers with inner and outer diameters of 3 and 9 nm, respectively; the complexes have alternating subunit stoichiometries of 3:4 and 4:3 between LukF and HS (*2*, *3*). The crystal structure of water-soluble monomeric LukF consists of cap, rim, and pre-stem domains (Fig. 1A), sharing a similar basic structure with a subunit (protomer) of the staphylococcal α-hemolysin homo-heptameric pore, except in the pre-stem domain (*4*, *5*). The LukF pre-stem domain folds back against the cap domain, while in α-hemolysin, it extends far into the lipid bilayer (*5*). These two structures suggest the beginning and ending points for a model of γ-hemolysin pore assembly, as follows: the rim domain for membrane binding, the β-sandwich (cap) domain for oligomerization with HS, and the pre-stem domain for the formation of pores through membranes (*4*). In our preceding study, the assembly of LukF and HS monomers into hetero-oligomers on the membranes of human red blood cells (HRBC) was clarified using a single-molecule fluorescence imaging technique (*6*). We estimated 11 sequential equilibrium constants for the assembly pathway, which includes initial membrane binding of monomers, single pore oligomerization, and finally the formation of clusters of pores. Nevertheless, the multiple functions of the individual domains of LukF, for example, the rim domain, during various stages of the pore assembly process have not yet been studied. Up to now, most studies have focused on the individual functions of domains; for example, 1) Y72 of the rim domain is a crucial residue for LukF binding to HRBC membranes (*7*), 2) S34 of the β-sandwich domain is essential for side-by-side interactions between LukF with HS to form oligomers (*6*), and 3) structural changes in the pre-stem domain are essential for pore-formation, but not for membrane-binding (*8–11*). Therefore, it is of interest to know if there are keys for such switching of the pre-stem domain. For a better understanding of the mechanism of spontaneous oligomerization and opening of the γ-hemolysin pore, we wanted to find, if there are any, key amino acids that do not directly participate in pore formation, but which can regulate this spontaneous stage. We looked for critical amino acids in the rim domain of LukF that function not only in membrane-binding, but also in later oligomerization stages. We also hoped to reveal multi-functional roles for the rim domain both in the membrane-binding and in the whole assembly process. For that purpose, we constructed 21 mutants, the amino acids located on the bottom surface of the LukF rim domain being replaced by either alanine or threonine, to identify residues that affect the hemolytic acivity of LukF (with HS). Mutations at the Y72, W177, R198, W257, F260, and Y261 residues (Fig. 1A and B) resulted in dramatic decreases in hemolytic activity of 5–10% compared to that of the wild-type LukF (detailed results for the Y72 mutation were published previously (*7*)). Interestingly, mutations at W177 and R198 resulted in about 5-fold lower membrane-binding activity compared with that of the wild-type LukF, as detected on Western immunoblotting, while the other four mutants (Y72A, W257A, F260A, and Y261A) almost completely lost the binding activity toward HRBC membranes. These four mutants were not suitable for studying critical amino acids for

*To whom correspondence should be addressed. Tel: +81-22-717-8779, Fax: +81-22-717-8780, E-mail: ykamio@biochem.tohoku.ac.jp

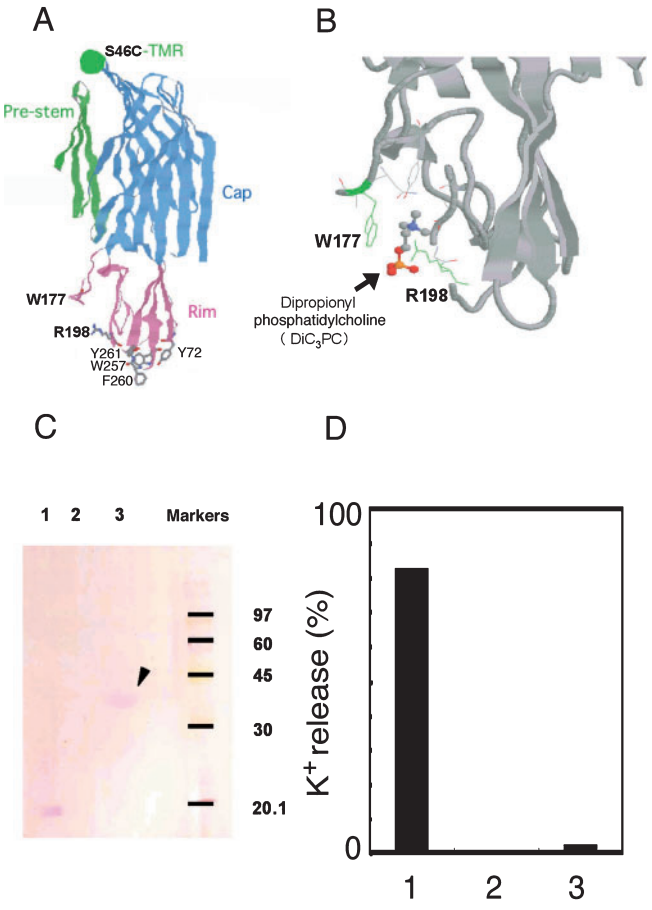

Fig. 1. **Mutation, labeling, and activity of the LukF mutant.** A: Three-dimensional structure of LukF. The cap (cobalt), pre-stem (green), and rim (violet) domains are indicated. The position of S46C for TMR fluorescence labeling is indicated by a green dot. W177 and R198, at the bottom of the rim domain of LukF, were selected for Thr substitutions. B: Close-up view of the model for the interaction between W177/R198 and the choline head group of PC. C: Detection of fluorescence labeling. The expression, purification, and labeling of W177T/R198T/S46C with TMR (W177T/R198T-TMR), as well as the preparation of LukF-TMR, LukF/S34C-TMR (LukF34-TMR), HS-IC5, and HS/T29C-IC5 (HS29-IC5) were performed as previously described (*6*). The degree of labeling for W177T/R198T-TMR was ~95%, as judged on measurement of the absorbance of TMR at 546 nm. The presence of free dye was negligible as no band of free dye was detected (lane 3). The specificity of the labeling at the Cys residues was confirmed by negative controls involving wild-type LukF (lane 2). Ten micrograms of fluorescent, TMR-labeled W177T/R198T-S46C protein was separated from free fluorescent dye on SDS-PAGE (lane 3, arrowhead); shown are the control of free dye alone (lane 1) and wild-type LukF treated with TMR-6-maleimide (lane 2). D: Potassium ion efflux by the wild-type (lane 1) and mutant (lanes 2 and 3). One % HRBC were incubated with LukF or W177T/R198T (1 μg/ml) and HS (1 μg/ml) (lanes 1 and 2), or W177T/R198T (10 μg/ml) and HS (10 μg/ml) (lane 3) at 37°C for 30 min, followed by centrifugation to obtain the supernatant for measuring K^+ efflux. The amount of potassium was determined using an atomic absorption spectrophotometer set at 766.5 nm (Hitachi A-2000). Full (100%) release was based on the concentration of K^+ released from cells exposed to 5 mM Tris-HCl (pH 7.4). Zero % release of K^+ was defined as the background K^+ level in the solution containing cells without the toxin.

pore formation as the initial binding stage did not occur. Thus, the W177 and R198 residues remained as candidates for studying effects on the later stages. In the previous study, we generated LukF mutants, named W177T, R198T, and W177T/R198T, in which W177, R198, and both the W177 and R198 residues were replaced by threonine (*7*). The W177T/R198T mutant never showed hemolytic activity with HS even at the extremely high protein concentration of 5 μM, whereas the wild-type LukF showed hemolytic activity at 1.36 nM. The single mutants, W177T/A and R198T, showed hemolytic activity (5–10% of the wild-type LukF) at the high protein concentration of 10 μg/ml (291 nM compared to 2 nM LukF for 50% hemolysis). In view of this, W177T/R198T is suitable for studying essential amino acids for the pore-formation stage of staphylococcal γ-hemolysin (data not shown). Here, we managed to examine "step-by-step" activities or the defective W177T/R198T mutant in the sequential stages of the pore assembly process, including membrane-binding, intermediate oligomerization, pore formation, and the formation of clusters of pores.

We created single-cysteine mutants, at S46 of W177T/R198T and at K222 of HS, and labeled them with fluorescence donors and acceptors, respectively, so that intermediate oligomers of the mutants could be detected by means of our recently-developed single-molecule imaging technique (*6*). The oligomerization of W177T/R198T with HS is indicated by the observation of fluorescence resonance energy transfer (FRET) between different dyes attached to W177T/R198T and HS. We examined an early stage of pore assembly, that is, membrane binding. To confirm maintenance of the three-dimensional structure of the mutant, circular dichroism (CD) analyses of the wild-type LukF, W177T/R198T and W177T/R198T/S46C were performed with a Jasco J-720 spectropolarimeter at room temperature in a 1-mm path length cell containing 5 μM protein in 5 mM potassium phosphate buffer (pH 6.5). The CD spectral profile of the mutant was similar to that of the wild-type LukF, indicating that the global structure of the mutant was not affected by the mutations (data not shown). The association constant K_{mF} for membrane-binding of the single-cysteine W177T/R198T/S46C mutant labeled with tetramethyl rhodamine (TMR) as a fluorescence donor (W177T/R198T-TMR; Fig. 1C) was calculated to be 10^{-5} μm^{-2}, by the method described previously (*6*) (Table 1), whereas K_{wF} for the wild-type was ~2×10^{-4} μm^{-2} (*6*). This demonstrates that the W177 and R198 residues play a role, though not a pivotal one, in the early stage of membrane-binding. Overall, based on the previous data obtained by us (*7*), and the model (*4*) of interactions between W177, R198 and dipropionylphosphatidylcholine (DiC_3PC) (Fig. 1B), we suspected that interactions between these two residues and membrane components including the choline head group may play a role in regulating the pore-assembly stages that lead to hemolysis of γ-hemolysin. Therefore, to determine if this mutant can undergo any further oligomerization steps or at which stage of pore assembly it stops, we detected intermediate oligomers formed by W177T/R198T-TMR and HS labeled with a fluorescence acceptor, IC5 (HS-IC5), under a single-molecule fluorescence microscope. The concentration of W177T/R198T-TMR was increased to 20 nM, compared to 1 nM LukF, in order

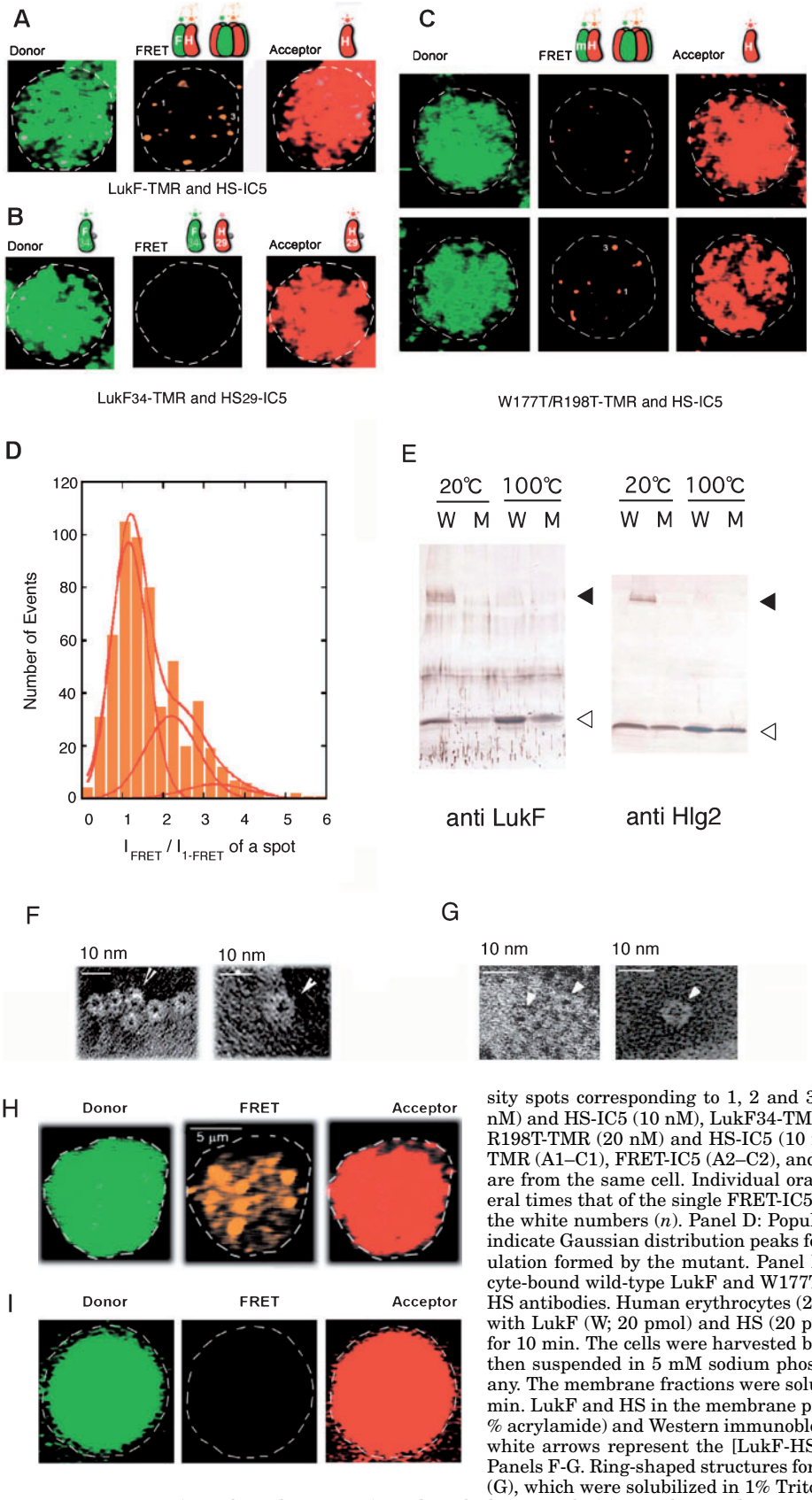

Fig. 2. **Visualization of oligomers formed by W177T/R198T and HS (Panels A–G), and visualization of clusters of pores (Panels H and I).** For single-molecule imaging of oligomerization, sample preparation, the total internal reflection fluorescent (TIRF)–microscopy, imaging, and data analysis were performed as described in the preceding paper (*6*). Briefly, 20 nM W177T/R198T-TMR and 10 nM HS-IC5 were both incubated with 1% HRBC in PBS at 25°C for 30 min. Samples containing toxin-bound ghost erythrocytes were observed under a TIRF-microscope (*6*, *12–14*). TMR and IC5 fluorophores (the fluorescence donor and acceptor) were excited with a Nd: YAG laser (Transverse Co., TIM-6222) at 532 nm and a He-Ne laser (Coherent Co., F44-30M) at 635nm, respectively. The objective (plan Apo ×60, N.A 1.4; Olympus Co.), dichroic mirrors (610 nm DM; Asahi Co.), 565–595 nm and 650–690 nm band-pass filters (580DF30, 670DF40; Omega Co.), and a SIT camera (Hamamatsu Photonics, C2400-08) were used to detect the dual signals of TMR and IC5. Adobe Photoshop was used for multi-color featured imaging. For calculation of association constants, the W177T/R198T mutant protein was assigned as ^{m}F to distinguish it from the ^{W}F, which was the assignation for the wild-type. Unit conversions for concentrations of proteins from molar to μm^{-2} membranes are shown as $[^{m}F_o] = [^{m}F'_o]/(120 \times [C'])$, where $[^{m}F_o]$ and $[^{m}F'_o]$ are the initial concentrations of W177T/R198T in μm^{-2} and M, respectively. One hundred and twenty μm^2 is the membrane area of one erythrocyte. $[C']$ is the cell concentration in M (1% cells = 6×10^{10} cells/liter = 0.1 pM). Association constants (μm^2) were estimated as described previously (*6*), as follows: $K_{(^{m}F \cdot H)} = [^{m}F \cdot H] \times [^{m}F_{-1}]^{-1} \times [H_1]^{-1}$. $K_{(^{m}F \cdot H)_2} = [(^{m}F \cdot H)_2] \times [^{m}F \cdot H]^{-1} \times [^{m}F \cdot H]^{-1}$. $K_{(^{m}F_3 \cdot H_{3-4})} = [^{m}F_3 \cdot H_{3-4}] \times [(^{m}F \cdot H)_2]^{-1} \times [^{m}F \cdot H]^{-1}$. where $[^{m}F_1]$ and $[H_1]$ (μm^{-2}) were obtained by dividing the total fluorescence intensity by the intensity of single monomers. $[^{m}F \cdot H]$, $[(^{m}F \cdot H)_2]$, and $[^{m}F_3 \cdot H_{3-4}]$ are the numbers of dimers, tetramers, hexamer/heptamers per μm^2, estimated based on the FRET-IC5 intensity spots corresponding to 1, 2 and 3 times $I_{\text{FRET-IC5}}$. Panels A–C: LukF-TMR (1 nM) and HS-IC5 (10 nM), LukF34-TMR (1 nM) and HS29-IC5 (10 nM), or W177T/R198T-TMR (20 nM) and HS-IC5 (10 nM) were incubated with 1% HRBC. Donor TMR (A1–C1), FRET-IC5 (A2–C2), and acceptor IC5 (A3–C3) signals, respectively, are from the same cell. Individual orange spots denote intensities which are several times that of the single FRET-IC5 value, indicated by $(^{m}F \cdot H)_n$, as indicated by the white numbers (n). Panel D: Population histogram of oligomers. The red lines indicate Gaussian distribution peaks for $^{m}F \cdot H$, $(^{m}F \cdot H)_2$, $^{m}F_3 \cdot H_{3-4}$, and the total population formed by the mutant. Panel E: Immunoblotting analysis of the erythrocyte-bound wild-type LukF and W177T/R198T, and HS using anti-LukF and anti-HS antibodies. Human erythrocytes (2×10^8 cells in 0.7 ml of PBS) were incubated with LukF (W; 20 pmol) and HS (20 pmol), or W177T/R198T (M) and HS at 37°C for 10 min. The cells were harvested by centrifugation at 8,000 × g for 10 min and then suspended in 5 mM sodium phosphate buffer (pH 7.4) to lyse intact cells, if any. The membrane fractions were solubilized with 1% SDS at 20°C or 100°C for 5 min. LukF and HS in the membrane preparations were analyzed by SDS-PAGE (8 % acrylamide) and Western immunoblotting as described previously (*8*). Black and white arrows represent the [LukF-HS]complex and LukF, W177T/R198T, or HS. Panels F-G. Ring-shaped structures formed by the wild-type (F) and W177T/R198T (G), which were solubilized in 1% Triton X-100, observed under a Hitachi electron microscope, H-8100 (Hitachi, Tokyo, Japan), as described previously (*3*). Panels H and I: W177T/R198T-TMR and HS-IC5 were applied to HRBC at 1,600 nM and 800 nM, respectively. In the case of LukF-TMR and HS-IC5, the concentrations were 40 and 400 nM. The laser power was adjusted to 1% power relative to that used in Fig. 2. No FRET signals were observed in the case of W177T/R198T (I), unlike the bright FRET region detected in the case of the wild-type (H).

to have an equal number of membrane-bound monomers for LukF and the mutant. The middle image in Fig. 2C shows various FRET-intensity spots formed by W177T/R198T-TMR and HS-IC5 scattered on the membrane. The individual FRET intensities were ~1, ~2 and ~3 times the intensity value for a single molecule. As was examined carefully in a preceding study (*6*), a single-FRET spot should represent a dimer containing 1 molecule of W177T/R198T-TMR and 1 molecule of HS-IC5; we assigned this as ${}^{m}F{\cdot}H$. The positive control, wild-type LukF, was confirmed by observation of various FRET-intensity spots (Fig. 2A). The negative control comprised the mutant LukF34-TMR and HS29-IC5, and showed the absence of any FRET-intensity spots due to the defective side-by-side interactions of these mutants (Fig. 2B) (*6*). If W177T/R198T-TMR and HS-IC5 form a dimer, ${}^{m}F{\cdot}H$, exhibiting single-FRET intensity, spots at relative intensities of ~2 should represent tetramers consisting of pairs of dimers $({}^{m}F{\cdot}H)_2$. Considering the heterodimers to be highly stable, the ~3 × single-FRET spots were resolved as hexamers $({}^{m}F{\cdot}H)_3$. However, it is also possible to resolve these spots as heptamers consisting of 3F and 4H because the FRET-IC5 intensity of oligomers is proportional to the number of donors if the acceptors are close to the donors. Thus, we assign the 3 × single-FRET as hexamer/heptamers, ${}^{m}F_3{\cdot}H_{3-4}$ (*6*). The population of each oligomeric intermediate was determined, and is presented as a histogram of FRET intensities (Fig. 2D). The histogram was the sum of three Gaussian distribution curves, in which the peak of spots at intensity ~3 was smaller than that of spots at intensity ~2. This is unlike the case of the wild-type, where the peak of the 3 × FRET spots is higher than that of the 2 × FRET spots. Assuming the area under each Gaussian curve is proportional to the number of oligomers, ${}^{m}F{\cdot}H$, $({}^{m}F{\cdot}H)_2$, and ${}^{m}F_3{\cdot}H_{3-4}$, we were able to estimate sequential association constants $K_{({}^{m}F{\cdot}H)}$, $K_{({}^{m}F{\cdot}H)_2}$, and $K_{({}^{m}F_3{\cdot}H_{3-4})}$ to be 0.00054, 9.4, and 5.8 μm^2, respectively (Table 1). $K_{({}^{m}F_3{\cdot}H_{3-4})}$ was slightly lower than $K_{({}^{m}F{\cdot}H)_2}$, suggesting that W177T/R198T did not assemble into stable hexamer/heptamers or, in other words, oligomerization to form hexamer/heptamers is not cooperative in the case of W177T/R198T and HS.

To ascertain whether or not the hexamer/heptamers are similar to normal pore structures, we observed isolated hexameric/heptameric complexes under a transmission electron microscope. When the membranes, which had been treated with HS and W177T/R198T, were solubilized in 1% Triton X-100, we observed several scattered ring-shaped structures with outer and inner diameters of 9 and 3 nm, similar to the structure of pores formed with wild-type LukF (Fig. 2F and G). But, if the membranes were solubilized in 1% SDS, we detected neither complexes of 195–240 kDa on SDS-PAGE (Fig. 2E) nor ring-shaped structures. At even when an extremely high concentration (5,000 nM) of the W177T/R198T protein was applied to 1% HRBC in the presence of HS, we did not observe significant potassium ion efflux through the pores with the double mutant, unlike with wild-type LukF (Fig. 1D). This value was ≥4,000 times of the concentration of wild-type (1.2 nM), which starts lysing HRBC (~1–2% hemolysis) (data not shown). Thus, W177T/R198T and HS could form ring-shaped structures with pre-pores which are unstable in SDS.

In the preceding paper, we mentioned that γ-hemolysin pores have a greater tendency to condense into clusters as the concentration of the toxin is increased, and may assemble into ≥3 pores because K_{3p} and K_{4p} were ~3 times higher than K_{2p} (*6*). This finding was supported by the previous data showing that large clusters of pores are observed with higher concentrations of proteins (1 μM) under a transmission electron microscope (*3*). Since clusters of pores are also observed with many other toxins, even in lipid vesicles (*15*), we suppose that the aggregation of pores is not only driven by the distribution of their receptors on membranes, but also by noncovalent linkages between amino acids located on the outer surfaces of the pores. One advantage of pore aggregation might be the switching of the equilibrium balance of single pore assembly toward association, thereby increasing the total number of pores per cell. Another advantage would be that large clusters of pores on the membranes weaken the cell membranes and enhance cell bursting. Electron microscopy of γ-hemolysin–treated erythrocytes revealed that the cluster formation of the pore complexes occurred together with hemolysis of human erythrocytes upon exposure of the cells to lower doses of the toxin, whereas the formation of single pore complexes was more strongly correlated with the swelling the cells. Thus, clustering of the pore complexes would cause intensive damage to the cell membranes in limited areas, leading to enhancement of hemolysis, and the cluster-forming ability of the pore complexes may be due to the asymmetric hetero-heptameric architecture, including the homodimeric linkage (*3*). Therefore, we examined if the ring-shaped hexamer/heptamers, which were defective in pores, can form clusters. We reduced the power of the excitation laser to 1% to achieve a linear response of the camera. While the wild-type formed clusters of pores, as indicated by bright FRET regions (Fig. 2H), there were no detectable bright FRET spots or regions even with 1,600 nM W177T/R198T and 800 nM HS (Fig. 2I), indicating that further cluster formation did not occur.

Taking the binding and three association constants into consideration (Table 1), we estimated the theoretical

Table 1. **Binding and association constants of intermediate stages in the pore assembly pathway.**

Constants for wild-type LukF (K_{wF})	Constants for mutant W177T/R198T (K_{mF})	Ratio K_{wF}/K_{mF}
2.1×10^{-4} (K_{wF})	10^{-5} (K_{mF})	21
0.0010 (K_{wFH})	0.00054 (K_{mFH})	1.8
3.1($K_{wF2\cdot H2}$)	9.4 ($K_{mF2\cdot H2}$)	0.3
37 ($K_{wF3\cdot H3-4}$ (K_p))	5.8 ($K_{mF3\cdot H3-4}$)	6.6
Totally multiplied ratio		75

Constants are given in units of μm^2. "w" in K_{wF} and "m" in K_{mF} denote the K_m values for the wild-type and mutant, respectively. The ratio K_{wF}/K_{mF} indicates the reduction in pore assembly efficiency caused by the mutation.

efficiency of hexamer/heptamer assembly for W177T/R198T to be ~75-fold lower than that for the wild-type (see Table 1). Assuming that hemolysis is proportional to the number of pores, the concentration of W177T/R198T for 50% HRBC (C50%) hemolysis should be 75 times $C_{50\%}$ for the wild type (4 nM), which is equal to ~300 nM. However, W177T/R198T neither caused K^+ efflux nor lysed HRBC (Fig. 1D). Therefore, the mutant hexamer/heptamers, which were unstable and could not further oligomerize into clusters, must be nonfunctional pores. As we observed that ring-shaped structures were formed by the mutant (Fig. 2G), it is possible that the hexamer/heptamers are defective because the pre-stem domain of LukF can not insert through the membranes. We conclude that interaction between W177 and R198 of the LukF rim domain and a special binding site on erythrocyte membranes is essential, functioning like a switch for the formation of pores. We also suggest that PC or its choline head group could be the special binding membrane component, as W177 and R198 are key residues for PC-binding.

We wish to thank Dr. Leslie Poole for critical reading of the manuscript. We also thank Dr. Kazuhiko Kimura for his help in measuring K^+ efflux. This work was supported by a Grant-in-Aid for Scientific Research from the Ministry of Education, Culture, Sports, Science and Technology of Japan (J.K., H.H. and Y.K.).

REFERENCES

1. Kamio, Y., Rahman, A., Nariya, H., Ozawa, T., and Izaki, K. (1993) The two Staphylococcal bi-component toxins, leukocidin and gamma-hemolysin, share one component in common. *FEBS Lett.* **321**, 15–18
2. Sugawara, N., Tomita, T., and Kamio, Y. (1997) Assembly of *Staphylococcus aureus* γ-hemolysin into a pore-forming ring-shaped complex on the surface of human erythrocytes. *FEBS Lett.* **410**, 333–337
3. Sugawara-Tomita, N., Tomita, T., and Kamio, Y. (2002) Stochastic assembly of two-component staphylococcal γ-hemolysin into heteroheptameric transmembrane pores with alternate subunit arrangements in ratios of 3:4 and 4:3. *J. Bacteriol.* **184**, 4747–4756
4. Olson, R., Nariya, H., Yokota, K., Kamio, Y., and Gouaux, E. (1999) Crystal structure of staphylococcal LukF delineates conformational changes accompanying formation of a transmembrane channel. *Nat. Struct. Biol.* **6**, 134–140
5. Song, L., Hobaugh, M.R., Shustak, C., Cheyley, A., Bayley, H., and Gauoux, E. (1996) Structure of staphylococcal α-hemolysin, a heptameric transmembrane pore. *Science* **274**, 1859–1866
6. Nguyen, T.V., Kamio, Y., and Higuchi, H. (2003) Single-molecule imaging of cooperative assembly of γ-hemolysin on erythrocyte membranes. *EMBO J.* **19**, 4968–4979
7. Yokota, K. and Kamio, Y. (2000) Tyrosine72 residue at the bottom of rim domain in LukF crucial for the sequential binding of the staphylococcal γ-hemolysin to human erythrocytes. *Biosci. Biotechnol. Biochem.* **64**, 2744–2747
8. Nguyen, T.V., Higuchi, H., and Kamio, Y. (2002) Controlling pore assembly of staphylococcal γ-hemolysin by low temperature and by disulfide bond formation in double-cysteine LukF mutants. *Mol. Microbiol.* **45**, 1485–1498
9. Valeva, A., Weisser, A., Walker, B., Kehoe, M., Bayley, H., Bhakdi, S., and Palmer, M. (1996) Molecular architecture of a toxin pore: a 15-residue sequence lines the transmembrane channel of staphylococcal alpha-toxin. *EMBO J.* **15**, 1857–1864
10. Valeva, A., Palmer, M., and Bhakdi, S. (1997) Staphylococcal alpha-toxin: formation of the heptameric pore is partially cooperative and proceeds through multiple intermediate stages. *Biochemistry* **36**, 13298–13304
11. Walker, B., Braha, O., Cheley, S., and Bayley, H. (1995) An intermediate in the assembly of a pore-forming protein trapped with a genetically-engineered switch. *Chem. Biol.* **2**, 99–105
12. Sako, Y., Minoguchi, S., and Yanagida, T. (2000) Single-molecule imaging of EGFR signalling on the surface of living cells. *Nat. Cell Biol.* **2**, 168–172
13. Funatsu, T., Harada, Y., Tokunaga, M., Saito, K., and Yanagida, T. (1995) Imaging of single fluorescent molecules and individual ATP turnovers by single myosin molecules in aqueous solution. *Nature* **374**, 555–559
14. Ishijima, A., Kojima, H., Funatsu, T., Tokunaga, M., Higuchi, H., Tanaka, H., and Yanagida, T. (1998) Simultaneous observation of individual ATPase and mechanical events by a single myosin molecule during interaction with actin. *Cell* **92**, 161–171
15. Wallace, A.J., Stillman, T.J., Atkinsm, A., Jamieson, S.J., Bullough, P.A., Green, J., and Artymiuk, P.J. (2000) *E. coli* hemolysin E (HlyE, ClyA, SheA): X-ray crystal structure of the toxin and observation of membrane pores by electron microscopy. *Cell* **100**, 265–276